Three-dimensional modelling of plasticity-induced crack closure in a 304L stainless steel: influence of crack length and crack shape.

C. Gardin[1,a], K. Vor[1,b], M. Arzaghi[1,c], C. Sarrazin-Baudoux[1,d] S. Fiordalisi[1,e] and J. Petit[1,f]

[1] Institut Pprime, CNRS-ENSMA UPR 3346 – Université de Poitiers – ENSMA, Téléport 2, 1 avenue Clément Ader, BP 40109, F86961 Futuroscope-Chasseneuil Cedex, France

[a] catherine.gardin@ensma.fr, [b] kokleang_vor@yahoo.com , [c] mandana.arzaghi@ensma.fr, [d] christine.baudoux@ensma.fr, [e] saverio.fiordalisi@ensma.fr, [f] jean.petit@ensma.fr

Keywords: Finite element modelling, plasticity-induced crack closure, stainless steel, short crack, crack shape.

Abstract. This paper addresses a precise investigation of the behaviour of physically short 2D cracks in condition where LEFM concepts are applicable. The influence of the plasticity-induced crack closure (PICC) on the global and local effective stress intensity factor is particularly investigated and modelled under constant ΔK amplitude loading in order to avoid any influence of loading history. Three-dimensional numerical models under Abaqus were used to determine the opening kinematics and to model the influence of crack length in the case of 2D through cracks with a straight crack front or a curved crack front.

Introduction

The concept of crack closure, consisting in a premature contact of the crack lips during cyclic loading, as initially proposed by Elber [1] is widely used to rationalize the propagation curves and has become one of the most intensively studied phenomena associated with fatigue crack growth. The closed crack is considered as non-effective for crack propagation. Therefore, the effective ΔK_{eff} (near tip) stress intensity factor range has been introduced to describe the effective driving force for crack propagation in condition of mode I crack opening. Consequently, characterization of closure has been intensively studied for long cracks. The higher crack growth rate of short cracks as compared to long cracks has been related in several cases to the lack of significant closure because of a small crack wake around crack lips [2-4]. When the LEFM conditions are satisfied, closure of short cracks has been shown to increase when cracks propagate, finally reaching the behaviour of long cracks [5, 6]. Suresh and Ritchie [3] suggested the following definitions by which short cracks can be broadly classified: i) crack whose size is comparable to the scale of the characteristic microstructural dimension is referred as microstructurally small cracks; ii) cracks for which the near-tip plasticity is comparable to the crack size are referred as mechanically small cracks; iii) fatigue flaws significantly larger than the characteristic microstructural dimension and the scale of the local plasticity are referred as physically short crack. Physically short cracks with initial dimensions larger than 3 to 5 times the average grain size, and when "far field" loading conditions allow the application of the linear fracture mechanic parameters, are relevant to the third type of this classification. This is the case of the cracks presently considered. The plasticity-induced crack closure (PICC) induced by constant stress intensity factor ranges is studied in a 304L stainless steel that undergoes high plasticity [7]. Three-dimensional simulations with both straight (for reasons of computing time) and circular curved fronts (for a better approximation of experimental observations of the real crack curvature) have been done to describe the influence of the length of 2D physically short cracks on the contribution of crack closure on the effective driving force.

Geometry of the model

The geometry modelled in this work corresponds to a CT-50 Compact Tension specimen with a thickness B=10mm, subjected to mode I loading. The analytical expression of the stress intensity factor is the following [8]:

$$K = \frac{F \times Y}{B\sqrt{W}} \text{ with } Y = \frac{(2 + a/W)\left(0.886 + 4.64(a/W) - 13.31(a/W)^2 + 14.72(a/W)^3 - 5.6(a/W)^4\right)}{(1 - a/W)^{3/2}} \quad (1)$$

where F is the applied load, a is the crack length. Here, w=50mm. Whatever the shape of the crack considered here, we will calculate K by using the edge crack length, as it is the one measured during tests via optical observations.

For symmetry reasons, only a quarter of the CT specimen has been modelled.

We impose here constant values of the stress intensity factor amplitude ΔK, with a stress ratio R=0.1. The load is imposed by applying cyclic pressure on a quarter of the two holes of the CT specimen.

We have used cubic linear elements, as generally used in 3D modelling [9, 10]. As important gradients of stresses and strains appear in the vicinity of the crack tip, the choice of element type and size of mesh is crucial, in order to obtain accurate results in a reasonable calculation time. The size of the elements should permit a precise characterization of the monotonic and plastic R_p zones. The minimum size proposed by Dougherty [11] is the following:

$$a_{\min} = \frac{1}{10} R_p = \frac{1}{10}\left[\frac{1}{2\pi}\left(\frac{K_{\max}}{\sigma_0}\right)^2\right] \quad (2)$$

Here, we have chosen a mesh four times smaller than that of the above recommendation. Different constant values of ΔK were studied, the minimum one being equal to $\Delta K = 12 MPa\sqrt{m}$ (leading to K_{max}=13,33 MPa√m, as R=0.1) which leads to element size in the direction of propagation equal to 0.05mm.

A mesh with 20 elements through the half thickness of the specimen, and with an increasing level of refinement towards the free surface (Fig. 1), has been retained, after a comparison with regular sizes in the thickness. Far from the crack, a considerably larger mesh is used.

In a first calculation, straight crack front has been considered, due to the simplicity reasons of its realisation. For reasons of calculation time, the maximum propagation *da* on the edge is 1.5mm, leading to 29 propagation steps, the initial crack length being equal to 0.1mm.

In order to approach experimentally observed crack shapes in these conditions of loadings, a propagation test alternatively performed in air and in vacuum has allowed us to reveal for long cracks, the transition air/vacuum, and the corresponding crack shapes (Fig. 2). For long cracks, the crack shape is almost independent of the crack length. It appears that an arc of circle allows an accurate description of the crack shape: the corresponding crack length in the heart of the CT specimen is then approximately 1mm longer than on the edge. A second mesh has then been considered: the different crack fronts regularly change from an initial straight crack front to an arc of circle after a propagation of 1.5mm, the final crack shape being close to the experimental one: for 1.5mm of propagation on the edge, the heart propagation is equal to 2.5mm. As a consequence, the crack length step is equal to 0.05mm on the edge and to 0.083 in the centre of the CT specimen.

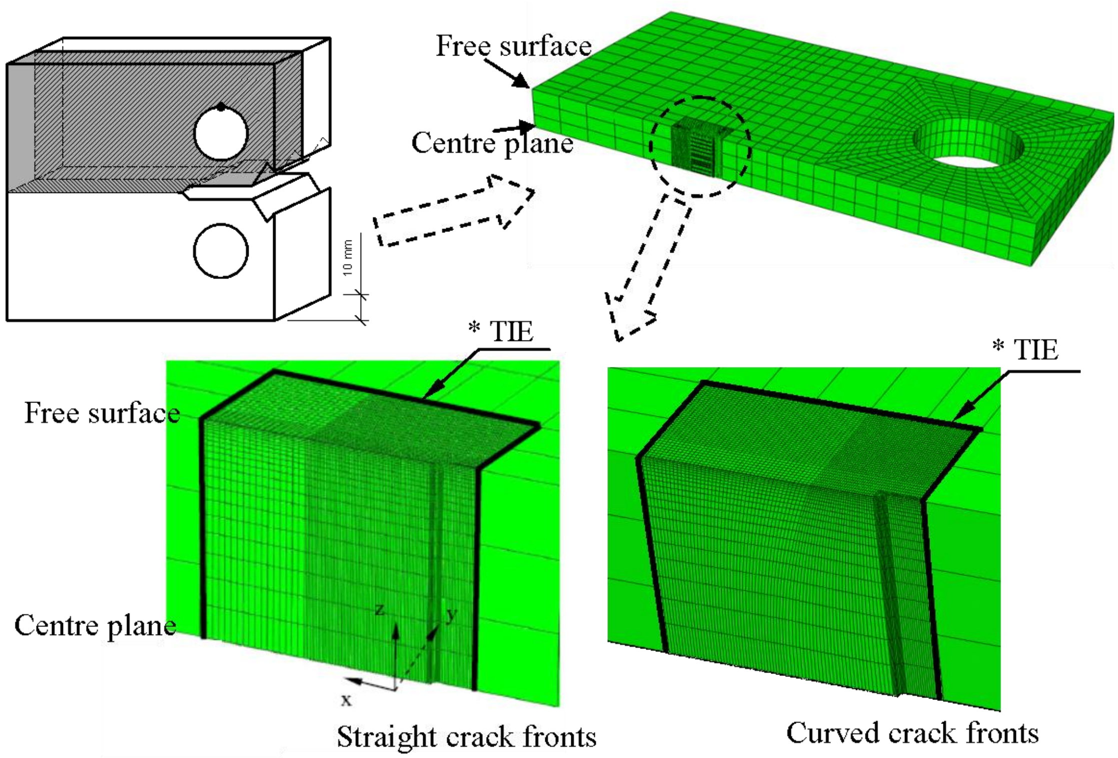

Fig.1. Mesh of a quarter of the CT specimen; zooms to clarify straight and curved crack fronts.

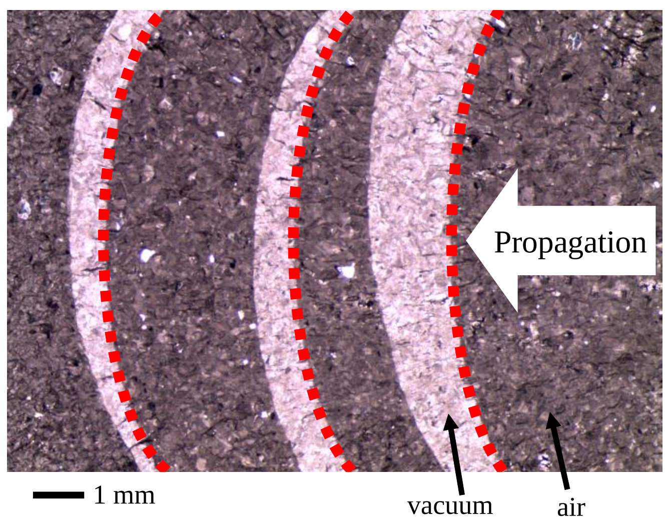

Fig.2. Examples of crack fronts obtained in 304L stainless steel, $\Delta K = 12 MPa\sqrt{m}$, R=0.1

Numerical modelling of crack propagation and plasticity-induced crack closure

Crack propagation schemes adopted here consist in releasing nodes for the current crack front, after applying a certain number of loading cycles. One crack growth increment corresponds to the size of the element ahead of the crack tip. In order to avoid numerical problems, releasing is performed at the minimum load. The number of cycles between releasing is a crucial parameter, especially for a material such as 304L stainless steel which presents strong hardening together with ratcheting. Here a combined isotropic and kinematic hardening law has been employed (Table 1). After various numerical tests, we finally performed 15 cycles between each releasing: this corresponds to an optimal solution taking into account the computational time.

Table 1. Coefficients used for the behaviour law of the 304L stainless steel studied

Elasticity		Kinematic hardening			Isotropic hardening		
E 196000 [MPa]	ν 0.3	σ_0 117 [MPa]	C 52800 [MPa]	D 300	σ_0 117 [MPa]	Q 87 [MPa]	b 9

The PICC is modelled by the contact of the crack flanks which is considered as a frictionless contact between the crack flank and an analytical rigid surface located in the crack propagation plane. The methodology is simple and enables easy determination of the local opening load P_{op} or opening SIF K_{op} (Fig. 3a). It is stated that local opening occurs when the monitored displacement perpendicular to the crack plane becomes positive during the loading stage of a cycle (fig. 3b).

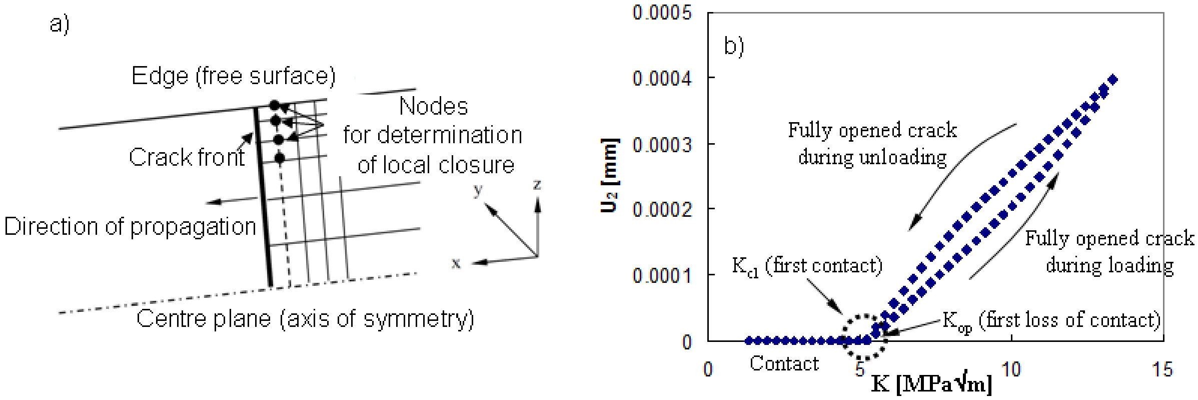

Fig.3. a) Location of the nodes allowing the determination of local crack closure b) determination of opening load P_{op}.

Results and discussion

Influence of the crack length and of the crack shape on the contact surface. Figure 4 shows the contact zones observed at the lowest applied load (R=0.1) for three different edge crack lengths (0.5, 1 and 1.5mm), and for both straight (upper figures) and curved (lower figures) crack fronts. The crack front is indicated by a dashed line on each figure. In all the situations, the major comment is that closure is concentrated on the edge of the specimens, where plane stress state prevails. The dimension of the contact zone in the thickness decreases during propagation, from 2 to 1 mm. The length on the edge reaches around 1.5mm at the end of the calculation. In the case of a curved crack front, the size of the contact zone in the thickness is close to 1.25mm. The contact surface is approximately twice smaller for curved cracks.

For straight crack fronts only, a small contact zone, corresponding to the size of one element (i.e. 0.05mm) is obtained for crack lengths of 0.5 and 1mm, but not for 1.5mm.

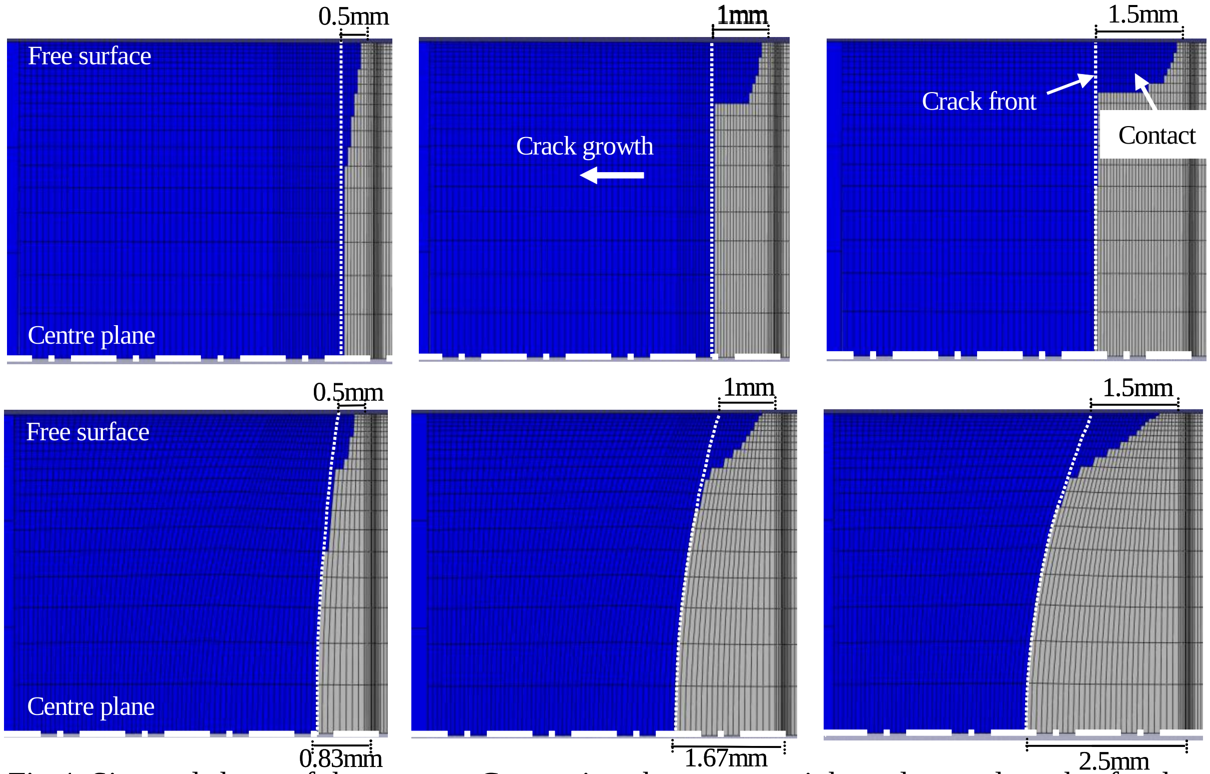

Fig.4. Size and shape of the contact. Comparison between straight and curved cracks, for three different crack lengths, and for $\Delta K = 12 MPa\sqrt{m}$, R=0.1

Local effective stress intensity factor range ΔK_{eff}. The Figures 5 a) and b) present the variations of K_{max}, K_{op} and ΔK_{eff} along the crack fronts, straight and curved, and for edge crack lengths equal to 0.5, 1 and 1.5 mm, for an applied value of loading equal to ΔK=12MPa.√m.

K_{max} is obtained by an elastic simulation at the higher applied load in accordance with the crack tip geometry. Through plastic calculations, K_{op} and ΔK_{eff} are obtained by the two following equations:

$$K_{op} = K_{\max} \frac{P_{op}}{P_{\max}} \tag{3}$$

$$\Delta K_{eff} = K_{\max} - K_{op} \tag{4}$$

where P_{op} is the load corresponding to local opening (Fig. 3b).

For straight crack fronts, K_{max} has the same evolution in the thickness for the three studied crack lengths. The computed average value of 13.3 MPa.√m is in agreement with the analytical expression, with constant values inside of the specimen close to 13.7 MPa.√m. A decrease of K_{max} is observed in near-edge area of about one millimeter, leading to a value of 11.4 MPa.√m at the edge. For curved crack fronts, K_{max} evolution is dependent on the front curvature. It is almost constant along the crack front for a=0.5mm but for larger cracks (a=1.5mm) and higher curvature, K_{max} becomes higher on the edges than in the heart of the specimen with a steady state value approximately close to 13.3MPa.√m. Finally, it comes out that for curved cracks, the average value of K_{max} is higher than 13.3MPa.√m, indicating that the analytical expression of K can be used only for straight cracks, i.e. under plane strain conditions.

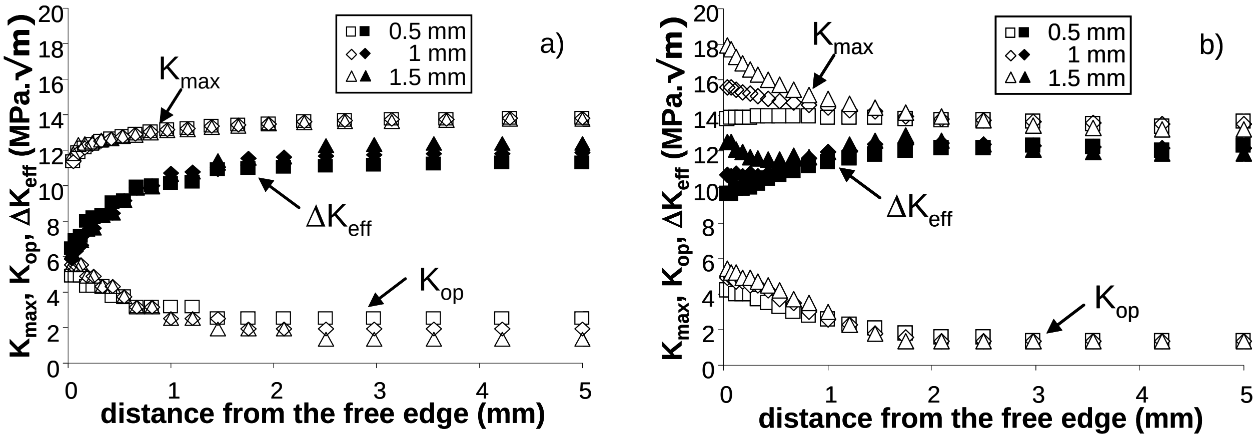

Fig.5. Variations of K_{max}, K_{op} and ΔK_{eff} along the crack front, for different edge crack lengths. a) straight cracks, b) curved cracks.

The corresponding K_{op} curves are very similar for the three crack lengths, for both straight and curved cracks. At the same time, crack closure is mainly observed (Fig. 5) through a thickness layer of 2 mm near the edge of the specimen. However, a small amount of closure is predicted in the heart of the specimen, only for short straight cracks.

For straight cracks, a progressive decrease of ΔK_{eff} is obtained from the heart to the edge of the specimen. Within the interval of crack length *da* here considered, variations of ΔK_{eff} with *da* are limited, but it can be noticed that the highest *da* value leads to the lowest ΔK_{eff} on the edge (6.2MPa.√m) in contrast with the highest in the heart [11.3 MPa.√m]. For curved cracks, the trend with respect to the crack length is comparable, but ΔK_{eff} evolution along the crack front through the specimen thickness is substantially different: for the smaller cracks (0.5 and 1mm), ΔK_{eff} is reduced on the edge but less reduced than for the straight crack front, and for da=1.5mm, ΔK_{eff} reaches approximately a constant value all along the front crack (the variation is about +/- 4%).

From these last results two major conclusions can be made:

- Firstly, a curved crack front induces an increase in K_{max} on the edge of the specimen while, even though for a larger crack length in the hearth of the specimen K_{max} is smaller;
- Secondly, the real crack curvature seems to result from the attainment of a constant ΔK_{eff} value all along the crack front, supporting that ΔK_{eff} is the true driving force for mode cracks in plane stress as well as in plain strain conditions, in contrast with the influence of these conditions on the closure contribution, which is much more enhanced in plane stress conditions.

One important consequence is that, when a global evaluation of closure and thus of ΔK_{eff} is performed by some global technique such as compliance variation, the measurement of ΔK_{eff} is pertinent since the value is the same all along the crack front. In such condition, a numerical simulation of the closure contribution through compliance variation is valuable.

Influence of the crack length on the global opening stress intensity factor K_{op}. The method based on the variation of compliance for crack closure determination by mean of a back face strain gage or/and a COD gauge mounted at the mouth of the notch, is simulated numerically by the displacement δ of the nodes corresponding to the gage position. The plotting of K versus δ' [12, 13], where $\delta' = \delta - \alpha K$, α being the compliance of the fully opening crack, then allows the determination of a global value of K_{op} for the specimen (Fig. 6) [14].

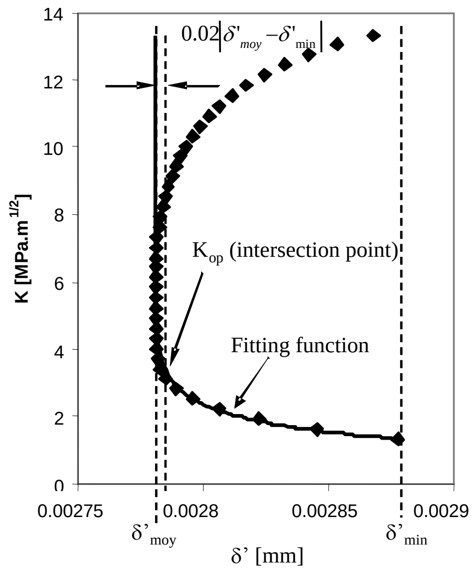

Fig.6. Compliance curve: K versus δ'. Schematic illustration of the method of determination of the global K_{op}

The numerical and experimental values [13] of global K_{op} versus crack length *da* are compared in Fig. 7 for three constant levels of applied constant ΔK (12 , 15, 18 MPa√m) under a stress ratio R=0.1. These values have been demonstrated to be equal to the one corresponding to the local opening at the edge of the specimen. As illustrated in Fig. 7, the numerical values of K_{op} obtained with an offset of 2% (as for experimental determination) are in a good agreement with the experimental measurements. The following results can be emphasized: first, a substantial increase in K_{op} with increasing *da* is shown for *da* lower than a critical length da_{cr} which is expected to define the boundary between the so-called short crack domain where K_{op} depends on *da*, from the long crack domain where K_{op} is constant and independent on *da*. The general trend of the observed evolution of K_{op} with respect to *da* is consistent with previous results provided by the literature for physically short cracks grown in condition where LEFM concepts can be used [15].

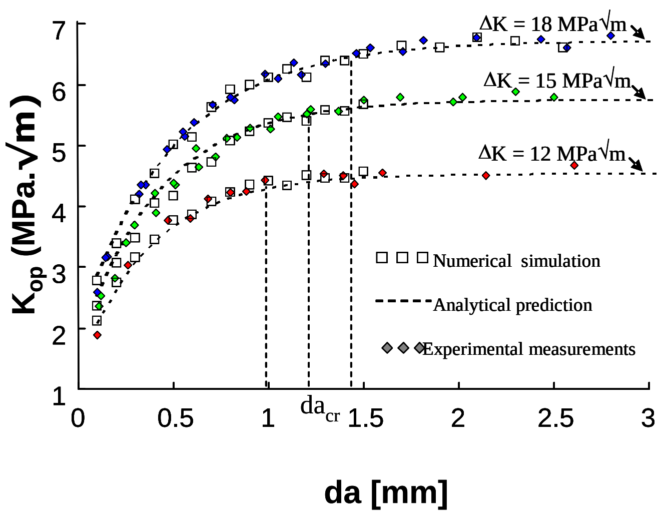

Fig.7. Evolution of K_{op} versus crack length: comparison between experiments and simulation (straight cracks) for three different values of constant ΔK applied

Conclusions.

From this 3D numerical simulation of plasticity-induced crack closure in a 304L austenitic stainless steel, the following concluding remarks can be drawn:

- For cracks lengths ranging between 0.1 and 1.5 mm, plasticity-induced crack closure as interpreted as the contact of the simulated crack flank with the rigid surface placed at the symmetry plane, is shown to result in a surface contact mainly localized near the edges of the specimen.
- The shape of the crack front in the specimen has a strong influence on the variations of K_{max} and K_{op} through the thickness. It seems, by comparison with experimentally obtained crack shapes, that ΔK_{eff} is the driving force for crack propagation.
- Numerical simulation of crack closure with respect to the crack length for crack grown at constant ΔK give a precise description of the increase of the contribution of crack closure with the crack length *da* when *da* is shorter than da_{cr} in the short crack regime, K_{op} being constant for long cracks.
- The specific effect of plasticity-induced crack closure has been clearly uncoupled from any other possible loading effect since tests and simulations are performed at constant applied ΔK range, so as to avoid any effect which could be generated by some ΔK variations related to the load history.
- Therefore, numerically simulated tests are very helpful to get more in-depth description and understanding of the fatigue crack growth mechanisms.

References

[1] W. Elber: Engng Fract. Mech. Vol. 2 (1970), p. 37-45.

[2] A.J. McEvily: JSME Int J. Vol. 32 (1989), p.181-191.

[3] S. Suresh and R.O. Ritchie: Int Metal Rev. Vol. 29 (1984), p. 445-476.

[4] H. Chang, E.H. Han, J.Q. Wang and W. Ke: Int. J. of Fatigue. Vol. 31 (2009), p. 403-407.

[5] J.L. Breat, F. Mudry and A. Pineau: Fat. and Fract. of Engng Mater. and Struct. Vol. 6(4) (1983), p. 349-358.

[6] A. Pineau: edited by J. Lankford, R.O. Ritchie, TMS AIME(1986), p. 191-209.

[7] S. Pommier: Int. J. of Fatigue. Vol. 25 (2003), p. 983-997.

[8] ASTM E647-1: Standard test method for measurement of fatigue crack growth rates. . ASTM Annual Book of ASTM Standards (2011).

[9] C.Y. Hou: Int. J. of Fatigue. Vol. 30 (2008), p. 1036-1046.

[10] K. Solanki, S.R. Daniewicz and J.C. Newman Jr: Engng Fract. Mech. Vol. 70 (2003), p. 1475-1489.

[11] J.D. Dougherty, J. Padovan and T.S. Srivatsan: Engng Fract. Mech. Vol. 56 (1997), p. 189-212.

[12] M. Kikukawa, M. Jono and S. Mikami: J. of the Soc. on Mat. Vol. 31 (1982), p. 438-487.

[13] K. Vor, C. Gardin, C. Sarrazin-Baudoux and J. Petit: submit. to Engng Fract. Mech. (2012)

[14] K. Vor, C. Gardin, C. Sarrazin-Baudoux and J. Petit: Revue de Métallurgie - Cahiers d'Informations techniques Vol. 107 (2010), p. 21-26.

[15] R.C. McClung RC and J.C. Newman Jr: in ASTM STP 1343 (1999).